Powder Technology 414 (2023) 118079

Contents lists available at ScienceDirect

Powder Technology

journal homepage: www.journals.elsevier.com/powder-technology

Numerical study of inlet eccentricity on liquid film spreading and splitting in centrifugal granulation assisted thermal energy recovery

Lei Peng [a,b], Long Li [a,b,*], Wei Zhao [a,b]

[a] State Key Laboratory of High Temperature Gas Dynamics, Institute of Mechanics, Chinese Academy of Sciences, Beijing 100190, China
[b] School of Engineering Science, University of Chinese Academy of Sciences, Beijing 100049, China

HIGHLIGHTS

- A simulation of centrifugal granulation under eccentric entry was carried out.
- Eccentric entry creates a new mode of liquid filament splitting.
- Consistent liquid film thickness and radial velocity distribution on the disc.
- A dimensionless particle size prediction equation with eccentricity was proposed.

GRAPHICAL ABSTRACT

The picture depicts the effect of eccentric inlet flow on liquid film spreading and edge splitting patterns on the disc during slag centrifugal granulation. This paper mainly introduced some regular information affected by operation parameters, eccentricity, and unstable working conditions

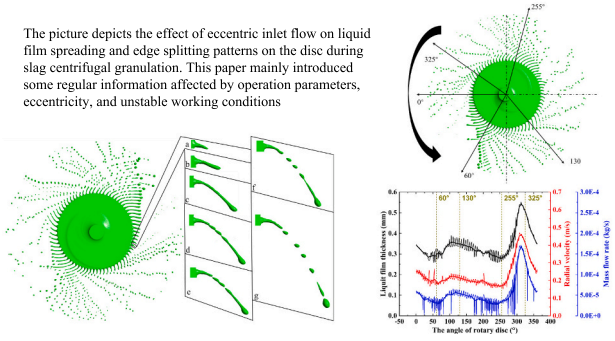

ARTICLE INFO

Keywords:
Rotating disc granulation
Simulation
Liquid filament splitting pattern
Particle size characteristics

ABSTRACT

Centrifugal granulation assisted thermal energy recovery(CGATER) is a method of recovering waste heat from molten slag by centrifugal granulation on a rotating disc. Disturbance and positioning errors can cause the incoming liquid column to deviate from the center of the disc. In this study, numerical simulation was conducted to investigate the effect of inlet eccentricity on liquid film flow spreading, liquid filament formation and fragmentation, and droplet size distribution during CGATER. The study shows that the eccentric granulation results in a new splitting pattern in which the liquid filament grows to a certain length with the rotation of the disc and then breaks from the bottom; the thickness of the liquid film on the eccentric granulation disc is consistent with the radial velocity distribution of the liquid film. Finally, the general dimensionless prediction correlation of particle median diameter is established for the eccentric situation.

1. Introduction

As one of the most serious energy-consuming industries in the world, the steel manufacturing process is accompanied by the production of blast furnace slag, which is discharged at a temperature range of 1450–1550 °C with thermal energy of about 1770 MJ/t. If discharged directly into the environment, it will cause huge energy waste and environmental pollution. [1] The traditional blast furnace slag water

Abbreviations: CGATER, Centrifugal granulation assisted thermal energy recovery.

* Corresponding author at: State Key Laboratory of High Temperature Gas Dynamics, Institute of Mechanics, Chinese Academy of Sciences, Beijing 100190, China.
E-mail address: lilong@imech.ac.cn (L. Li).

https://doi.org/10.1016/j.powtec.2022.118079
Received 26 September 2022; Received in revised form 3 November 2022; Accepted 4 November 2022
Available online 9 November 2022

quenching method will not only consume a lot of water resources and will release toxic and harmful gases into the atmosphere, the heat of high-temperature slag cannot be effectively used. Dry granulation of blast furnace slag can alleviate these problems and reduce energy consumption, which is important for sustainable economic development [2].

The wind quenching technique, rotating drum method, mechanical stirring method, and CGATER method were all suggested and developed as a result of the dry granulation and heat recovery of blast furnace slag research that began in the 1970s [3,4]. The CGATER method was proposed by Yoshinaga et al. [5], in Japan in 1982. The basic principle is to use a high-speed rotating disc or cup to make the liquid slag under the action of centrifugal force granulated into small droplets, and with air for direct or indirect efficient heat transfer quickly solidified into slag particles. This technology can theoretically obtain small particle size slag with high glass phase content, which is an excellent raw material for cement, and the waste heat recovery rate of slag is over 90%.

Although the method for granulating molten blast furnace slag liquid into droplets using the centrifugal force generated by the spinning of a rotating disc or rotating cup is rather straightforward, the mechanism for spreading and rupturing the molten slag liquid film in it is quite complex. Early scholars mainly used experimental methods to study this process, Yoshinaga et al. [5], Pickering et al. [6] and Kashiwaya et al. [7] conducted experimental studies on CGATER of rotating discs, cups, and cylinders, respectively. Wu et al. [8], Peng et al. [9], and Wang et al. [10] experimentally investigated the effects of fluid flow, viscosity, and rotating speed of the rotating disc on the granulation splitting pattern as well as the droplet particle size distribution. Using molten tin and aluminum as the experimental fluids, respectively, Xie et al. [11] and Peng et al. [12] investigated the impact of various granulator surface morphologies on the particle diameter of granulation and discovered that these morphologies affect the concentration of atomized particle size. Tan et al. [13] used a mixture of water and glycerol as the experimental fluid and found that the lateral morphology of the disc has a huge effect on the droplet splitting pattern. They [14] also proposed a novel stacked rotary cup atomizer (SRCA) in 2021, and experimentally found that the SRCA has good granulation performance under high flow rate conditions to produce smaller particles and suppress slagging. Tan et al. [15] and He et al. [16,17] respectively, added blast air holes and water curtain around the rotating cup, which increased the liquid filament instability and accelerated the solidification of slag particles.

Due to the rapid development of computational fluid dynamics, which makes the numerical study with the advantages of low cost and short time consumption, many scholars have studied the centrifugal granulation flow field flow and the relationship between particle size and granulation conditions by numerical simulation. For example, Pan et al. [18,19] studied the effect of high-temperature slag on liquid film thickness by 2D numerical simulation with different parameters of inlet flow rate, rotational speed, and disc diameter, and summarized the dimensionless relationship between droplet diameter and liquid film thickness. By using the order of magnitude analysis to simplify the N-S equation, Wang et al. [20,21] was able to determine the liquid layer thickness and radial velocity at every radial point on the disc. They then confirmed their results using a 2D numerical simulation. For the investigation of the movement of liquid film on the disc's surface, Li et al. [22] simulated the water flow spreading process on the rotating disc through large eddy simulation and observed the formation and development of unstable waves of liquid film on the surface of the disc, which is in good agreement with the experimentally taken photos. For the study of adding a cooling device around the granulator, He et al. [23] proposed the rapid cooling of granulated ferroalloy powder by arranging a water curtain at the edge of a porous rotating cylinder, numerically simulated the temperature change history of ferroalloy powder in air and water curtain. Gao et al. [24,25] studied the effect of different disc edge morphology on the particle size distribution and simulated the effect of disc edge blast air on CGATER. They found that the particle size

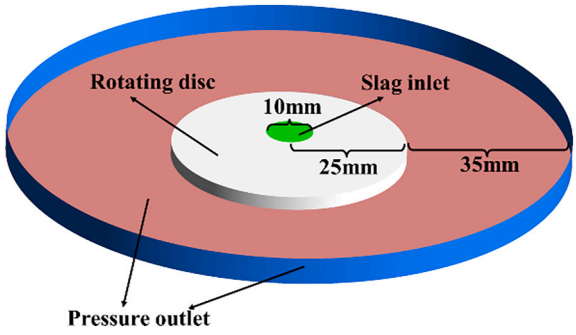

Fig. 1. Computation domain and boundary conditions of the physical model.

was reduced, and the particle size uniformity was better within a certain blast airspeed. Mantripragada et al. [26] used 3D numerical simulation to study the three splitting modes—drop, filament, and film—along with a phase change model to explore the temperature distribution throughout the flight of individual droplets.

In summary, there are many experimental and numerical studies for central centrifugal granulation, but in practice, perturbation and positioning errors can cause the incoming liquid column to deviate from the center of the granulator. Li et al. [27] and Xu et al. [28] studied the effect of eccentric inflow on the rotary cup granulation by simulation, and obtained the distribution of liquid film thickness and particle size distribution in the rotary cup under different eccentricity rates. The impact of eccentric inflow on the granulation effect has, however, hardly ever been studied for the most basic granulator, the disc. The present study used numerical simulation to describe the CGATER process of the disc in order to explore the impact of eccentric inflow on liquid film flow spreading and liquid filament formation fragmentation. Investigated were the effects of various eccentricities on liquid film thickness, radial velocity, and droplet diameter distribution. In order to direct the centrifugal granulation operation of a high-temperature slag carousel, the general dimensionless prediction correlation of particle median diameter was finally summarized.

2. Methodology

2.1. Physical model

With a high-temperature slag liquid inlet diameter of 10 mm, a disc diameter of 50 mm, and a total calculation domain diameter of 120 mm, a 3-D model (Fig. 1) was built for numerical computation in the current study. The following presumptions were made to streamline the model. (1) Ignoring the impact of heat transmission since the liquid slag had a limited range of temperature drops during the spreading and granulation stages. Existing simulation studies had tested this assumption and found it to be plausible [20,24,25,29]. (2) Since the flow velocity of the slag and surrounding air was substantially lower than the speed of sound during granulation, it was assumed during the simulation that the two fluids were incompressible. (3) It was assumed that the liquid slag was continually poured at a constant temperature and flow rate, despite the fact that the process really included parameter variations.

2.2. Mesh division

The top surface area of the disc and the annular granulation region were the two components of the computational domain that were partitioned throughout the meshing process. The mesh was indicated in Fig. 2, with the two parts connected at the edge of the disc by a non-common node. Setting the grid adaptive approach in the calculation allowed for the liquid filaments and droplets produced during the granulation process to be captured.

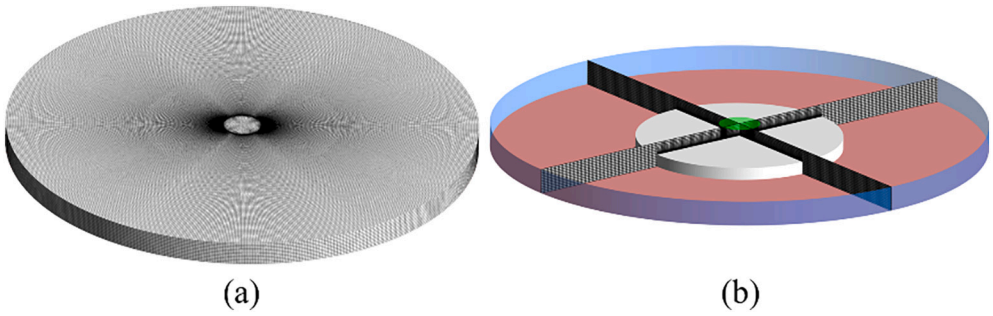

Fig. 2. Mesh division: (a) overall mesh, (b) section mesh.

2.3. Governing equations

The VOF (Volume of Fluid) method, a versatile and successful interface tracking technique based on the idea of fluid volume, was utilized to precisely capture the flowing liquid film on the disc's surface as well as the liquid filaments and droplets in the granulation zone during the computation process. The core idea of this method is that incompatible fluid components share a set of control equations, and the tracking of phase interfaces in the fluid computational domain is achieved by introducing the variable of phase volume fraction α_q. α_q represents the ratio of the volume of one of the phases to the volume of the grid in which it is located, and is mathematically described as shown in Eq. (1).

Table 1
Physical properties of granulated materials.

Materials	Density (kg/m^3)	Dynamic viscosity (Pa • s)	Surface tension(N/m)
Slag	2590	$5.12\times10^{-9}e^{\frac{18992.64}{T}}$	$0.789-(1.484\times10^{-4})T$
Air	1.225	1.789×10^{-5}	

Where σ_{ij} is the surface tension, the subscript i and j denote the gas phase and liquid phase, respectively. k_i is the surface curvature, which is defined by the divergence of unit normal $\hat{n}$, and the equations are described as follows:

$$\begin{array}{ll} \alpha_q = 1 & \text{All A}-\text{phase in the grid} \\ 0 < \alpha_q < 1 & \text{The grid contains two phases A and B, with the phase interface between the two} \\ \alpha_q = 0 & \text{All B}-\text{phase in the grid} \end{array} \quad (1)$$

The value of α_q in each grid is derived by calculating the continuity equation for the volume fraction of each phase, and the location of each phase interface is identified. The continuity equation for the volume fraction of each phase is illustrated in Eq. (2).

$$\frac{\partial \alpha_q}{\partial t} + \nabla\left(\vec{v}\alpha_q\right) = 0 \quad (2)$$

The physical parameters within the grid of the control body cell are calculated using a weighted average of the physical volume fractions of each phase, for example, the density within the cell is given by:.

$$\rho = \sum \alpha_q \rho_q \quad (3)$$

The mass and momentum equations in the control equation are shown:

$$\frac{\partial \rho}{\partial t} + \frac{\partial(\rho u)}{\partial x} + \frac{\partial(\rho v)}{\partial y} + \frac{\partial(\rho w)}{\partial z} = 0 \quad (4)$$

$$\frac{\partial(\rho \vec{u})}{\partial t} + \nabla \bullet (\rho \vec{u}\vec{u}) = -\nabla p + \nabla \bullet [\mu(\nabla \vec{u})] + \rho \vec{g} + \vec{f} \quad (5)$$

In the above equation ρ is the density. $\vec{u}$ is the velocity vector. μ is the dynamic viscosity. $\vec{g}$ is the acceleration of gravity. $\vec{f}$ are other volume force source terms. In the VOF calculation model, the gas-liquid surface tension is reflected in the momentum equation in the form of volume force source terms, whose expressions are shown:

$$f_{vol} = \sigma_{ij}\frac{\rho k_i \nabla \alpha_i}{\frac{1}{2}(\rho_i + \rho_j)} \quad (6)$$

$$k = \nabla \bullet \hat{n}\,\hat{n} = \frac{n}{|n|} \qquad n = \nabla\alpha \quad (7)$$

The SST k-ω model, which takes turbulent shear stress transport into account, has shown to be more accurate and dependable over a wider range of flows and is also effective at describing CGATER processes. The following equations can be used to get the turbulent kinetic energy k and the specific dissipation rate w.

$$\frac{\partial(\rho k)}{\partial t} + \frac{\partial}{\partial x_i}(\rho k u_i) = -\overline{u_i' u_j'}\frac{\partial u_i}{\partial x_j} + \frac{\partial}{\partial x_j}\left[\left(\mu + \frac{\mu_t}{\sigma_k}\right)\frac{\partial k}{\partial x_j}\right] - \beta^* \rho k \omega \quad (8)$$

$$\frac{\partial(\omega)}{\partial t} + \frac{\partial}{\partial x_i}(\rho \omega u_i) = \frac{\partial}{\partial x_j}\left[\left(\mu + \frac{\mu_t}{\sigma_\omega}\right)\frac{\partial k}{\partial x_j}\right] + 2(1-F_1)\frac{\rho}{\omega \sigma_\omega}\frac{\partial k}{\partial x_j}\frac{\partial \omega}{\partial x_j}$$

$$-\beta \rho \omega^2 - \frac{\alpha \alpha^*}{\nu_t}\overline{u_i' u_j'}\frac{\partial u_i}{\partial x_j} \quad (9)$$

In the above equation β^*, β, α and α^* are constants, μ_t is the turbulent viscosity. σ_k and σ_ω are the turbulent Prandtl numbers of k and ω, respectively. F_1 is the first mixing function in the turbulence model.

3. Results and discussion

3.1. Model validation

The slag granulation process under centrosymmetric conditions was first calculated using a BF slag liquid inlet mass flow rate of 2 kg/min, a disc speed of 1780 rpm, and the BF slag and air physical parameters as shown in Table 1 [24,30]. Three meshes with different numbers (mesh

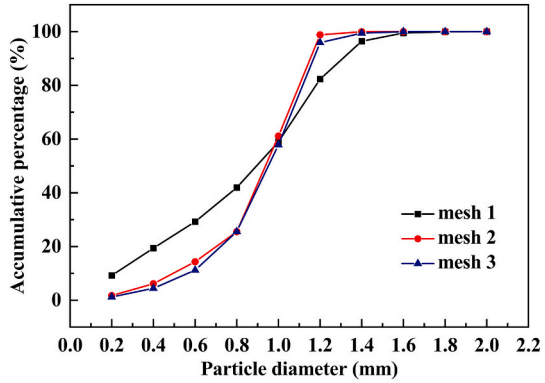

Fig. 3. Particle size distribution under different grid conditions.

1: 830000, mesh 2:1220000,mesh 3: 1830000) were adopted to carry out the grid-free independence test. Capturing the liquid phase in the simulation process using grid adaption method. The numbers of the three sets of grids after grid adaption during the calculation are 1.39 million, 1.96 million and 2.52 million, respectively. Particle size sampling was carried out once the granulation process had reached a generally smooth stage. The droplet diameter statistics are divided into three steps: 1) visualize and analyze the calculated results and export the liquid phase diagram of the flow field; 2) import the liquid phase diagram into the image recognition software Image J and convert the image into a binarized image according to the threshold; 3) the software automatically calculates the droplet area data according to the scale in the image, and then converts it into diameter data. Processing 20 liquid phase figures from different moments of simulation at a time, with droplet numbers in the range of 6000–10,000. The results are shown in Fig. 3. After fully considering the calculation accuracy and computational cost, mesh 2 was selected as the model for this simulation grid.

The calculated results were then compared with the experimental findings reported by CSIRO [20] as shown in Fig. 4 to confirm the accuracy of the numerical method. According to the comparison findings, the grid adaption in the annular granulation domain might capture the gas-liquid interface more precisely, which resulted in a higher degree of agreement between the simulated flow field and the actual condition. The simulated results deviate somewhat from the experimental liquid filament amount. This is due to the fact that the experimental procedure will create vibration during the rotation of the motor and disc, which would worsen the breakage of the liquid filament, resulting in a lower number of liquid filaments than the estimated number in the vibration-free simulation.

To further compare the consistency of simulation and experimental results, the simulated particle size distribution was compared with the CSIRO experimental data as shown in Fig. 5a. The difference between the particle size distribution and the experimental results is primarily due to the fact that the vibration during the rotation of the motor and disc during the experimental process causes the liquid filament to break when it is thicker and shorter, resulting in larger diameter particles.At the same time, because the experimental process there will be liquid film does not spread the phenomenon of the direct splash, thus causing the formation of large diameter particles. The comparison showes that the simulated slag particle size distribution is more concentrated, but the

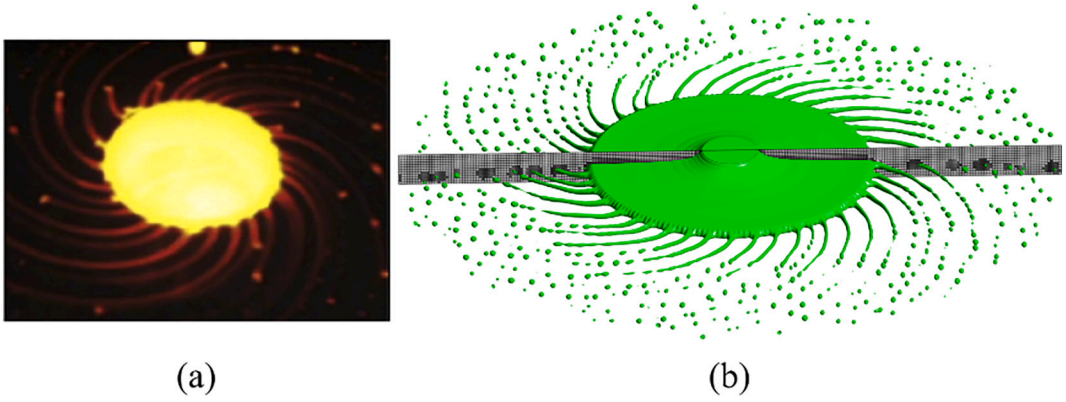

Fig. 4. Comparison of central granulation results: (a) CSIRO [20] experimental granulation flow field (b) simulation of granulation flow field.

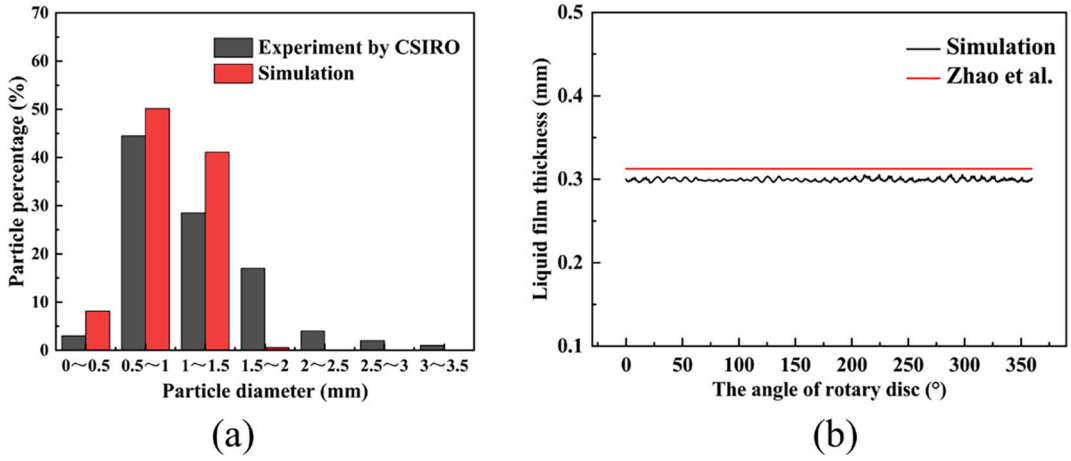

Fig. 5. Model verification diagram: (a) Comparison of the experiment by CSIRO and simulation, (b) Comparison of the results by Zhao et al. and simulation.

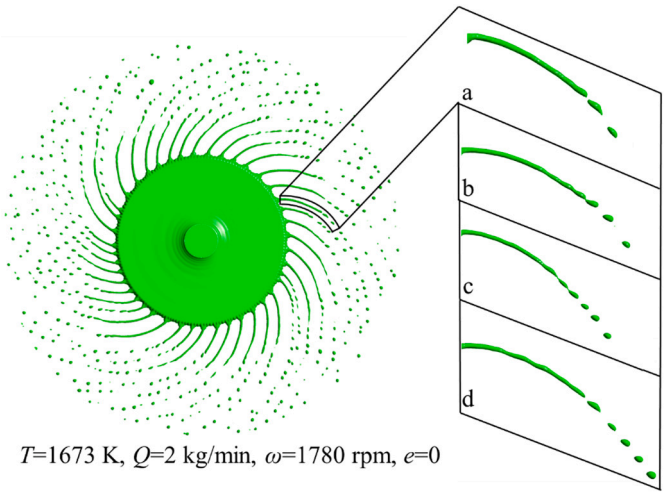

Fig. 6. Liquid filament breaking to form droplets under non-eccentric condition, at T = 1673 K, Q = 2 kg/min, ω = 1780 rpm, e = 0.

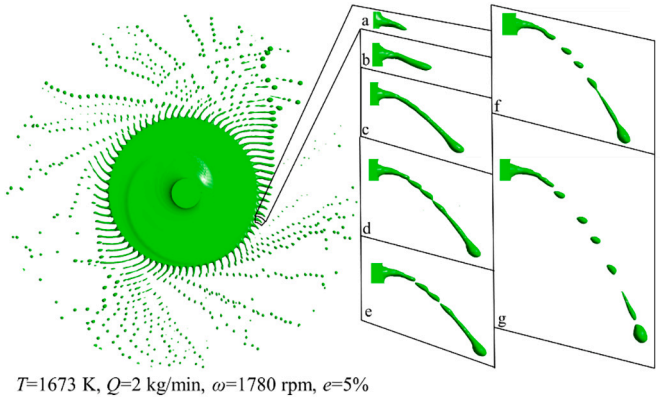

Fig. 7. Liquid filament breaking to form droplets under 5% eccentricity, T = 1673 K, Q = 2 kg/min, ω = 1780 rpm, e = 5%.

two particle size distribution trends are consistent. A comparison of the liquid film thickness distribution at the edge of the disc with the results of Zhao et al. [31] is shown in Fig. 5b, and it can be seen that they are in good agreement. The accuracy of the numerical model is verified to a certain extent.

3.2. Effect of eccentricity on droplet splitting pattern

Keeping the inlet mass flow rate, disc rotational speed, disc diameter, and physical properties the same as the CSIRO [20] experimental parameters, the CGATER process was simulated for an inlet eccentricity of 5% (eccentricity distance of 1.25 mm). The eccentricity e is calculated as follows, where e is the eccentricity, l is the distance from the center of the inlet to the center of the disc, and R is the radius of the disc.

$$e = l/R \times 100\% \tag{10}$$

Comparing the droplet splitting without eccentricity and 5% eccentricity, as shown in Fig. 6 and Fig. 7, respectively. Under the center-inflow situation, the liquid film spreads evenly on the disc and subsequently forms a liquid filament that is stretched at the disc's edge by centrifugal force. The velocity of the liquid film in the flow process will not match with the air flow velocity, resulting in disturbances that form K—H instability, while the liquid filament will form R-T instability when moving in the air. These disturbances will spread and grow along the outside of the liquid filament, and eventually cause breakage at the top

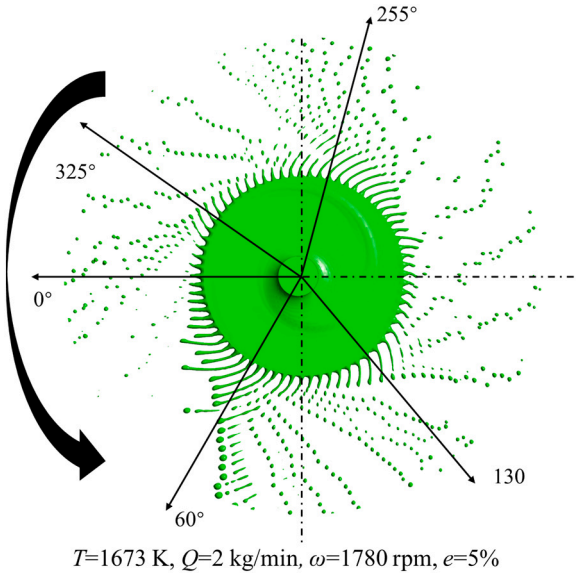

Fig. 8. Coordinates and rotation direction of 5% eccentricity granulation flow field, at T = 1673 K, Q = 2 kg/min, ω = 1780 rpm, e = 5%.

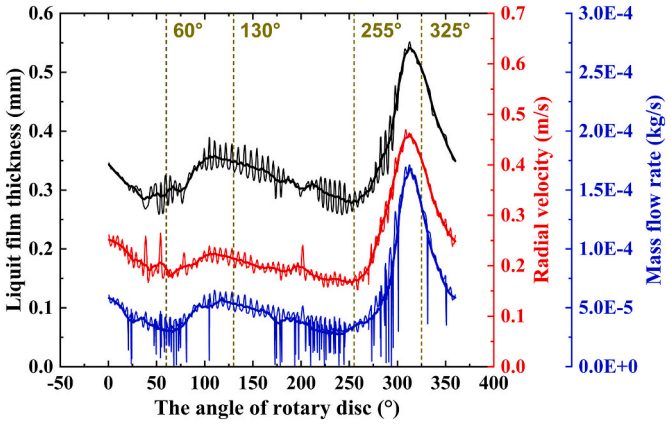

Fig. 9. Variation of characteristic parameters of liquid film at different positions on the edge of 5% eccentricity granulation disc, at T = 1673 K, Q = 2 kg/min, ω = 1780 rpm, e = 5%.

of the liquid filament to form droplets. There is only one mode of droplet formation in the case of no eccentricity, that is after the liquid film forms a liquid filament at the edge of the disc, the tip of the liquid filament is broken to form a droplet; while droplet formation in the condition of inflow eccentricity not only has the mode of breaking the tip of the liquid filament but also appears breakage from the root of the liquid filament. The main reason for the breakage of the bottom end of the filament is the uneven distribution of the liquid film caused by the eccentric entry flow, resulting in the accumulation of more liquid flow at the head of the filament that starts to form in the thicker area of the liquid film. The liquid filament will go through the thin liquid film area when it rotates with the rotating disc, and the final formed liquid filament will be thicker at the top and thinner at the bottom of the liquid filament. The instability will cause the liquid filament to break from the thinner bottom end.

The coordinates and direction depicted in Fig. 8 were established on the disc to more effectively investigate the eccentricity phenomena. The 0° line indicates the direction of the line linking the disc's center and the center of the incoming flow, and the coordinate origin is the disc's center. The disc rotates counterclockwise. The findings demonstrate that the eccentricity, which causes considerable filament growth and bottom

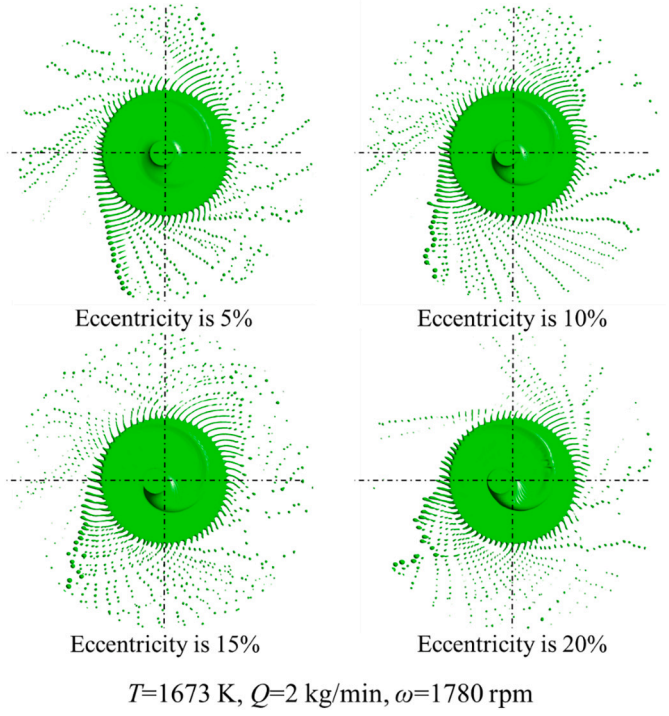

Fig. 10. Effect of different eccentricity on granulation effect, at $T = 1673$ K, $Q = 2$ kg/min, $\omega = 1780$ rpm.

breakage, is what produces the uneven length of liquid filaments near the disc's edge. At 0°, the filament is short and grows with the rotation of the disc, and rarely the droplet breaks from the tip of the filament. At 60°, the long liquid filament starts to break at the bottom end, breaking again in the air to form droplets.

There are four processes of liquid filament growth and fracture from the 0° line in the granulation zone of the rotary disc. At angles of 60°, 130°, 255°, and 325°, respectively, the fractures happen. In comparison to those at 130° and 325°, the liquid filaments that break at 60° and 255° are longer. Fig. 9 displays the distribution of liquid film thickness, radial velocity, and mass flow rate at various locations along the disc's edge. The thick solid line in the middle represents the oscillation curve after it has been smoothed. As can be observed, the liquid film thickness is obviously raised at 310°, which is due to the convergence of the liquid flow near the liquid flow inlet on the surface of the disc due to the eccentricity of the inlet flow. During the rotation of the disc, most of the converged liquid flow will be spread to the edge of the disc in the form of a spiral line, which eventually forms a bulge in the liquid film thickness.

There is a new phenomenon is that the distribution of radial velocity and liquid film thickness at the disc's edge is consistent, and the greater the liquid film thickness, the higher the radial velocity and the greater the mass flow rate at the edge. The main reason for this phenomenon is that the eccentricity causes the converging liquid flow to flow on the disc for different times. The thicker the liquid flow, the longer the flow distance on the disc and the acceleration time, the greater the radial velocity, and ultimately the greater the flow rate.The four times of liquid wire breaking at the bottom end are all near the maximum or minimum value of mass flow, which indicates that the eccentricity of slag inflow will directly lead to uneven mass flow distribution at various positions on the rotary disc, and the maximum and minimum values of flow will occur at the edge of the rotary disc. The accumulated liquid flow in the area between the maximum and minimum values of flow will make the liquid filaments grow slowly and break after the extremum value of flow.

3.3. *Influence of different eccentricity*

To further investigate the effect of eccentricity on the granulation, the granulation results were simulated for inlet eccentricities ranging from 5% to 20% while keeping other granulation conditions consistent, as shown in Fig. 10. Increasing the eccentricity will lead to an increased disturbance on the disc, making it easier for the filament to shatter during the growth process, with shorter filament lengths at the edge of the disc.

The liquid film data on the upper surface edge of the disc at different eccentricities are shown in Fig. 11. It is clear that under center-inflow

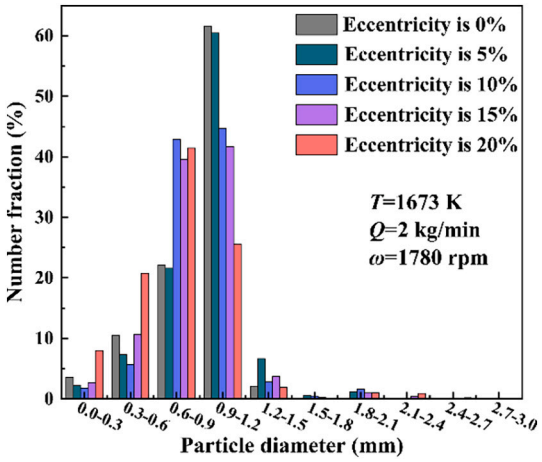

Fig. 12. Particle size distribution under different eccentricity, at $T = 1673$ K, $Q = 2$ kg/min, $\omega = 1780$ rpm.

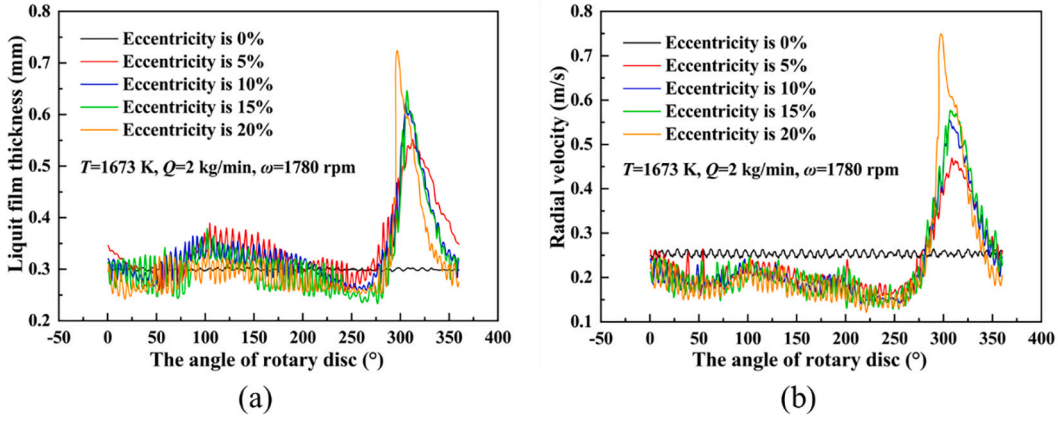

Fig. 11. Comparison of liquid film thickness and radial velocity distribution at the edge of the disc, at $T = 1673$ K, $Q = 2$ kg/min, $\omega = 1780$ rpm.

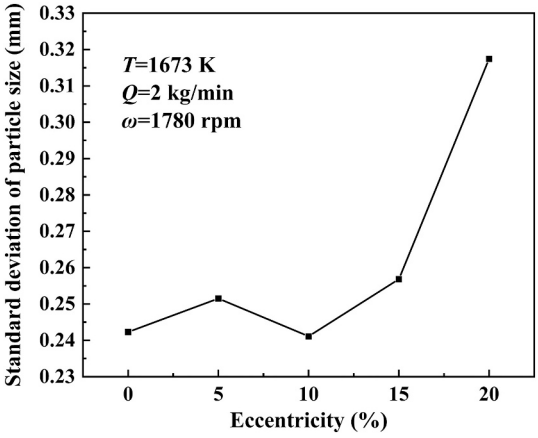

Fig. 13. The standard deviation of particle size at different eccentricity, at T = 1673 K, Q = 2 kg/min, ω = 1780 rpm.

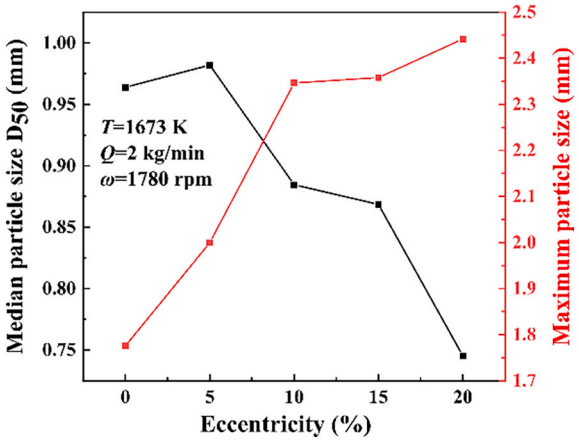

Fig. 14. Variation of median particle size and maximum particle size at different eccentricity, at T = 1673 K, Q = 2 kg/min, ω = 1780 rpm.

conditions, the liquid film thickness and radial velocity distribution of centrifugal granulation are relatively uniform. Eccentricity leads to uneven distribution of the liquid film on the disc, producing a fluid convergence effect. The fluid convergence effect is more pronounced the bigger the eccentricity. The maximum liquid film heights at the corresponding eccentricity ratios of 5%, 10%, 15%, and 20% were 0.552 mm, 0.622 mm, 0.644 mm, and 0.724 mm, respectively. As a result, the liquid film thickness increased by 80.5%, 103.6%, 111.6%, and 136.9%, respectively, in comparison to the case without eccentricity. The maximum radial velocities of the liquid film for each eccentricity were 0.470 m/s, 0.556 m/s, 0.577 m/s, and 0.749 m/s, respectively, which were higher than the radial velocities without eccentricity by 77.4%, 110%, 118.1%, and 183.1%.

When the eccentricity is small, there will be multiple extreme points of flow at the edge of the disc. As the eccentricity increases, the extreme points of flow decrease, and the positions of liquid filament breaking at the bottom decreases accordingly. The eccentricity has no significant effect on the trend of liquid film position distribution, only exacerbating the degree of liquid film convergence.

The diameter distribution and standard deviation of granulated droplets as shown in Fig. 12 and Fig. 13. As can be observed, when there is little or no eccentricity, the particle size standard deviation is lower and the particle size distribution is more concentrated. As the eccentricity increases, the standard deviation of particle size increases, the concentration of particle size becomes worse and the proportion of small diameter droplets increases. This is because when the incoming flow's

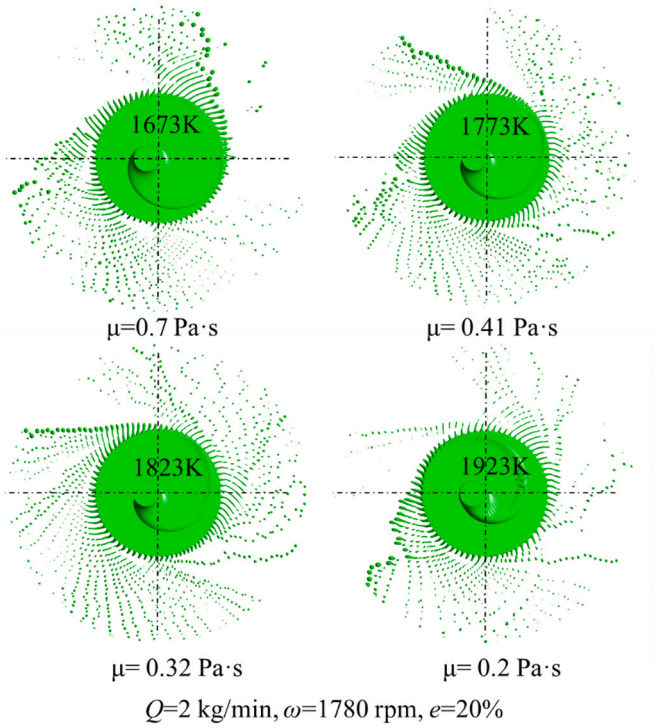

Fig. 15. Granulation effect of slag liquid at different temperatures, at Q = 2 kg/min, ω = 1780 rpm, e = 20%.

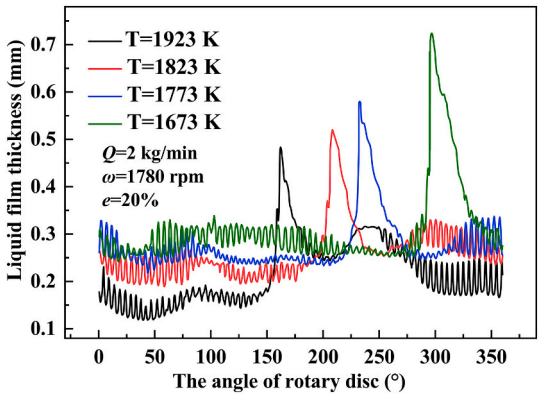

Fig. 16. Liquid film height distribution at different slag temperatures, at Q = 2 kg/min, ω = 1780 rpm, e = 20%.

eccentricity rises, more areas of thin liquid film zones form on the disc, resulting in the granulation-produced droplet size at the borders of these film areas decreasing.

Fig. 14 depicts the variation of median particle size and maximum particle size at various eccentricities. It can be observed that the two exhibit opposing tendencies as eccentricity increases. At 20% eccentricity, the maximum particle size grows by 37.5% while the median diameter decreases by 22.7% when compared to the case without eccentricity. This is because a large eccentricity leads to a thicker film and smaller area in the thick liquid film region, which produces fewer and larger droplets; and a thinner film and larger area in the thin liquid film region, which produces more and smaller droplets.

3.4. Effect of granulation parameters on eccentric granulation results

3.4.1. Effect of temperature

In this study, the effect of eccentric granulation of slag at different

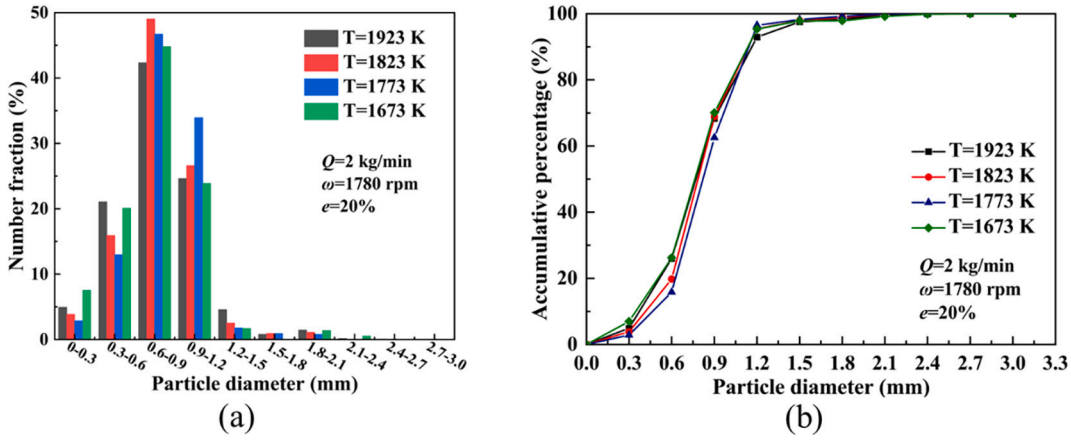

Fig. 17. Granulation particle size statistics at different slag temperatures: (a) percentage of different intervals, (b) accumulative percentage of quantity, at $Q = 2$ kg/min, $\omega = 1780$ rpm, $e = 20\%$.

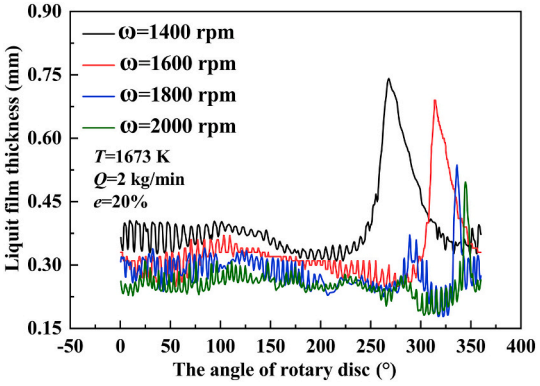

Fig. 18. Liquid film height distribution at the edge of the disc at different speeds, at $T = 1673$ K, $Q = 2$ kg/min, $e = 20\%$.

temperatures was investigated. The eccentric granulation of slag at four different temperatures was simulated under the condition that the eccentricity was guaranteed to be 20% and the disc speed was 1780 rpm, respectively. The density essentially does not change when the temperature rises from 1673 K to 1923 K, and the surface tension only decreaces from 0.54 to 0.5, while the viscosity falls from 0.7 to 0.2. To simplify the simulation, only the effect of viscosity for the change of physical parameters caused by temperature change is considered in this study [24,30]. The simulation results (Fig. 15) show that there are two fragmentation modes of bottom filament breakage and tip splitting for all four temperatures of droplet splitting, demonstrating that a temperature change does not affect the splitting mode. By comparing the liquid film height distribution at the edge of the disc (Fig. 16), it is found that as the slag temperature increase, the liquid viscosity decrease and the liquid film thickness become thinner. When the temperature increases from 1673 K to 1923 K, the height of the film's highest point decreases from 0.724 mm to 0.483 mm, and the relative deviation from the 0° position angle decreases from 296.93° to 162.01°.

According to Fig. 17, which depicts the granulation particle size distribution at various slag temperatures, it can be seen that the temperature has less of an impact on the distribution of particle sizes. This finding is consistent with the findings of Gao's [24] study, and it may be because viscosity has less of an impact on the process by which liquid filament-forming droplets fracture.

3.4.2. *Effect of rotational speed*

An increase in rotating speed causes a reduction in particle size during center-entry granulation. This study evaluated the eccentric granulation of disc speeds between 1400 and 2000 rpm at a guaranteed flow rate of 2 kg/min and a granulation temperature of 1673 K to study the impact of rotational speed on eccentric granulation. It is found that the liquid film thickness at the edge of the disc decreases as the speed

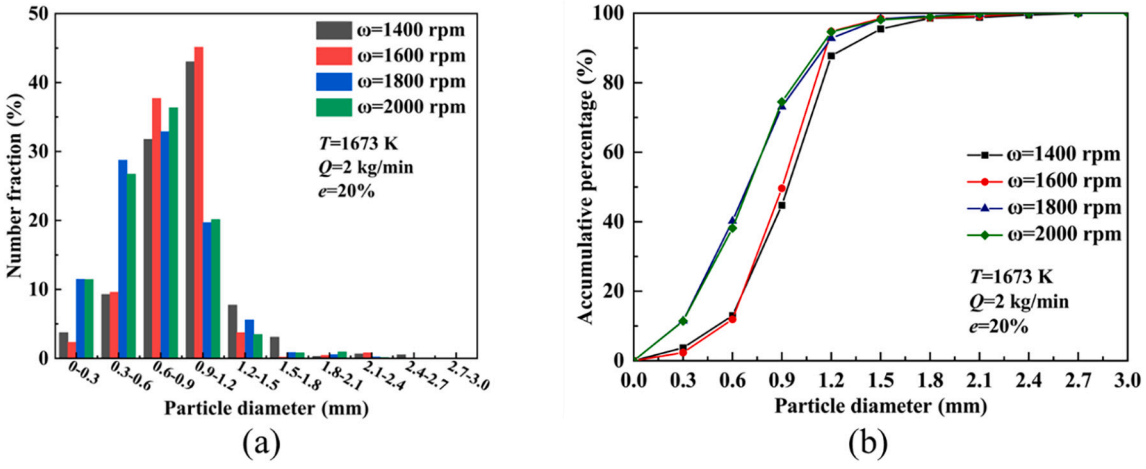

Fig. 19. Granulation particle size statistics at different turntable speeds: (a) percentage of different intervals, (b) accumulative percentage of quantity, at $T = 1673$ K, $Q = 2$ kg/min, $e = 20\%$.

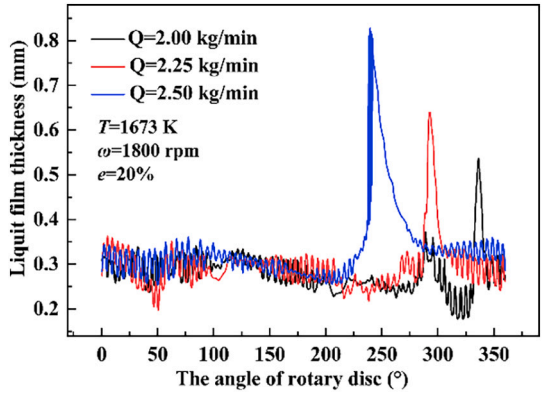

Fig. 20. Liquid film height distribution at the edge of the disc at different flow rates, at $T = 1673$ K, $\omega = 1800$ rpm, $e = 20\%$.

increases (Fig. 18), the height of the liquid film aggregation point decreases, and the angle of deviation from the 0° position increases. The reason for this phenomenon is that the increase in speed leads to an increase in centrifugal force, an increase in liquid film flow rate, and a decrease in liquid film thickness at a certain total flow rate.

As the speed increases, the particle size distribution shifts towards smaller particle sizes (Fig. 19), on the one hand, because the liquid film is thinner, on the one hand, the centrifugal force increases, making the liquid filaments more prone to breakage.

3.4.3. Effect of different flow rates

The effect of the flow rate (2 kg/min to 2.5 kg/min) on the granulation of the eccentric slag was calculated numerically with a guaranteed speed of 1800 rpm and a granulated slag liquid temperature of 1673 K. Fig. 20 shows that increasing the flow rate increases the height of the liquid film aggregation point and decreases the angle of deviation of the liquid film apex position from the 0° line, but does not have a significant effect on the height of the liquid film in other regions. Fig. 21 shows that as the flow rate increases, the number of large diameter droplets increases.

3.5. Regression analysis

The particle size prediction equations proposed in the existing CGATER studies are mainly described using the interrelationships of Reynolds number *Re*, Weber number *We* and Onetzog number *Oh* [8,24,32,33], which are calculated as shown below, respectively.

$$Re = \frac{4\rho Q}{\pi \mu R} \tag{11}$$

$$We = \frac{\rho \omega^2 R^3}{\sigma} \tag{12}$$

$$Oh = \frac{\mu}{\sqrt{\rho \sigma R}} \tag{13}$$

In the above equation, ρ is the density of slag, Q is the volume flow rate of slag, μ is the dynamic viscosity, R is the radius of the disc, ω is the rotational speed of the disc, σ is the surface tension.

In this study due to the eccentricity of the incoming flow, the eccentricity *e is* introduced in the particle size prediction equation. By nonlinearly fitting the median diameter data obtained from the above eccentric granulation calculations, a particle size calculation formula with eccentricity is obtained to be applicable for practical engineering applications. Fig. 22 compares the distribution results of the particle size calculated by the fitted formula with that obtained by numerical simulation under the same working conditions, and it is found that the median particle size obtained by numerical simulation has a good correlation with Eq. (14) for a large number of data points, and the maximum error of the predicted formula is 11%, and the application range of the fitting formula is $5\% \le e \le 20\%$, $2.425 \le Re \le 8.488$, $1819.723 \le We \le 3713.72$, $0.036 \le Oh \le 0.126$.

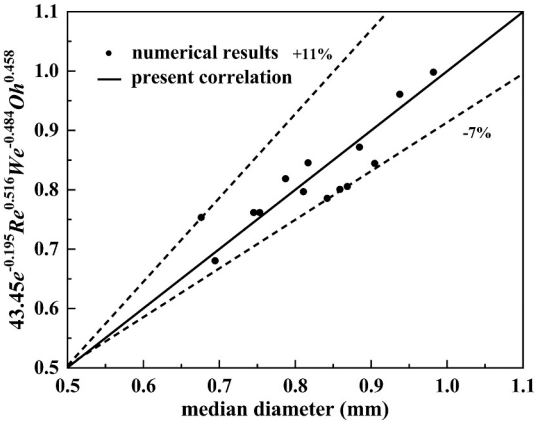

Fig. 22. Median diameter comparison between numerical simulation and fitted formula calculation.

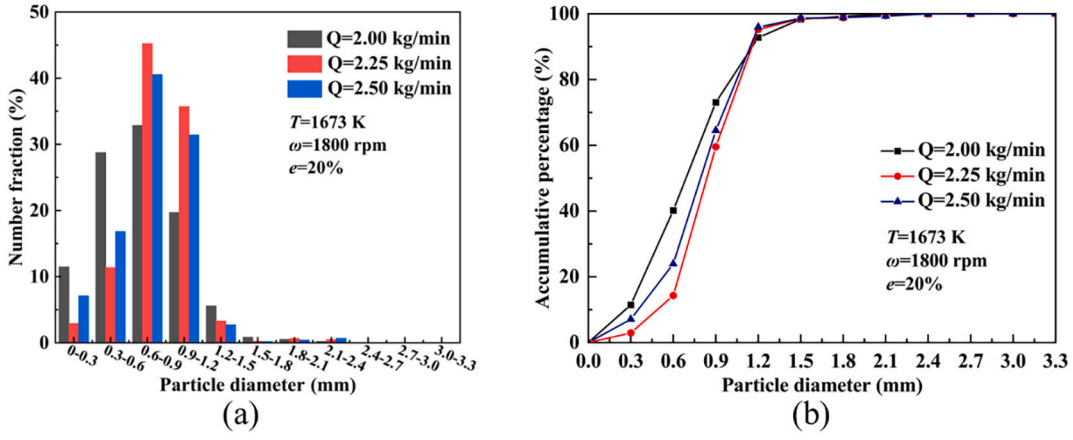

Fig. 21. Statistics of granulated particle size at different flow rates: (a) percentage of different intervals, (b) accumulative percentage of quantity, at $T = 1673$ K, $\omega = 1800$ rpm, $e = 20\%$-.

$$\frac{d}{R} = 1.738e^{-0.195}Re^{0.516}We^{-0.484}Oh^{0.458} \quad (14)$$

4. Summary

In this study, the eccentricity effect of CGATER of high-temperature slag prepared by rotating disc was simulated by establishing a three-dimensional model. By comparing the central inflow, it is found that the eccentric inflow causes uneven distribution of the liquid film on the disc surface and changes the droplet splitting pattern as well as the particle size distribution. The main research conclusions are as follows:

1) The eccentric granulation will change the droplet splitting mode, not only has the traditional central granulation has the top of the filament broken split, but also has a short filament growth to the long filament and then broken at the bottom, broken into droplets in the air of the new splitting mode.

2) The distribution of liquid film thickness on the eccentric granulation disc is consistent with the distribution of liquid film radial velocity. The thicker the liquid film, the higher the radial velocity at the edge, and thus the larger the mass flow rate. The location of the long liquid filament breaking from the edge is similar to the location of the extreme value of the liquid mass flow rate.

3) The greater the eccentricity, the greater the unevenness of the liquid film distribution on the disc and the decrease in the length of the granulated liquid filament. At the same time, the larger the eccentricity, the more dispersed the particle size distribution, the larger the proportion of small diameter droplets, the smaller the median value of particle size, and the larger the maximum value of particle size.

4) With the same eccentricity, increasing the disc speed or decreasing the slag flow rate will result in a larger proportion of small diameter droplets for granulation, making the median size of the granulated droplets decrease. However, changing the slag granulation temperature, i.e., changing the slag viscosity, has no significant effect on the particle size distribution of the granulated droplets.

5) A dimensionless median particle size prediction equation with eccentricity was established for the following ranges: $5\% \le e \le 20\%$, $2.425 \le Re \le 8.488$, $1819.723 \le We \le 3713.72$, $0.036 \le Oh \le 0.126$. The maximum error between the predicted and simulated values in this interval is 11%, which provides some guidance for engineering design.

CRediT authorship contribution statement

Lei Peng: Conceptualization, Data curation, Writing – original draft, Software. **Long Li:** Methodology, Formal analysis, Writing – review & editing. **Wei Zhao:** Visualization, Investigation, Supervision.

Declaration of Competing Interest

The authors declare that they have no known competing financial interests or personal relationships that could have appeared to influence the work reported in this paper.

Data availability

The data that has been used is confidential.

Acknowledgment

The authors gratefully acknowledge the financial support from the Youth Fund of State Key Laboratory of High Temperature Gas Dynamics, Institute of Mechanics, Chinese Academy of Sciences (QN20210004).

References

[1] H. Zhang, H. Wang, X. Zhu, Y.J. Qiu, K. Li, R. Chen, Q. Liao, A review of waste heat recovery technologies towards molten slag in steel industry, Appl. Energy 112 (2013) 956–966, https://doi.org/10.1016/j.apenergy.2013.02.019.
[2] L.Y. Wang, W.Q. Sun, X.L. Li, J.J. Cai, Flight dynamics and sensible heat recovery of granulated blast furnace slag, Open Fuels Energy Sci. J. 8 (2015) 356–360, https://doi.org/10.2174/1876973X01508010356.
[3] M. Barati, S. Esfahani, T.A. Utigard, Energy recovery from high temperature slags, Energy. 36 (2011) 5440–5449, https://doi.org/10.1016/j.energy.2011.07.007.
[4] G. Bisio, Energy recovery from molten slag and exploitation of the recovered energy, Energy. 22 (1997) 501–509, https://doi.org/10.1016/S0360-5442(96)00149-1.
[5] M. Yoshinaga, K. Fujii, T. Shigematsu, T. Nakata, Dry granulation and solidification of molten blast furnace slag, Trans. Iron. Steel Inst. Jpn. 22 (1982) 823–829, https://doi.org/10.2355/isijinternational1966.22.823.
[6] S.J. Pickering, N. Hay, T.F. Roylance, G.H. Thomas, New process for dry granulation and heat recovery from molten blast-furnace slag, Ironmak. Steelmak. 12 (1985) 14–21, https://doi.org/10.1016/0304-386X(85)90024-6.
[7] Y. Kashiwaya, Y. In-Nami, T. Akiyama, Development of a rotary cylinder atomizing method of slag for the production of amorphous slag particles, ISIJ Int. 50 (2010) 1245–1251, https://doi.org/10.2355/isijinternational.50.1245.
[8] J.J. Wu, H. Wang, X. Zhu, Q. Liao, B. Ding, Centrifugal granulation performance of liquid with various viscosities for heat recovery of blast furnace slag, Appl. Therm. Eng. 89 (2015) 494–504, https://doi.org/10.1016/j.applthermaleng.2015.06.031.
[9] H. Peng, N. Wang, D.X. Wang, X. Ling, Experimental study on the critical characteristics of liquid atomization by a spinning disk, Ind. Eng. Chem. Res. 55 (2016) 6175–6185, https://doi.org/10.1021/acs.iecr.6b00401.
[10] D.X. Wang, X. Ling, H. Peng, Z.W. Cui, X.J. Yang, Experimental investigation of ligament formation dynamics of thin viscous liquid film at spinning disk edge, Ind. Eng. Chem. Res. 55 (2016) 9267–9275, https://doi.org/10.1021/acs.iecr.6b01428.
[11] J.W. Xie, Y.Y. Zhao, J.J. Dunkley, Effects of processing conditions on powder particle size and morphology in centrifugal atomisation of tin, Powder Metall. 47 (2004) 168–172, https://doi.org/10.1179/003258904225015482.
[12] H. Peng, X.K. Shan, X. Ling, D.X. Wang, J. Li, Analogue experimental investigation on ligament granulation of molten slag in various rotary disk configurations for waste energy recovery, Results Phys. 11 (2018) 385–393, https://doi.org/10.1016/j.rinp.2018.09.037.
[13] Y. Tan, H. Wang, X. Zhu, Y.W. Lv, X.Y. He, Q. Liao, On the centrifugal granulation characteristics by rotary disk: effect of outer edge structure, Appl. Therm. Eng. 159 (2019), 113977, https://doi.org/10.1016/j.applthermaleng.2019.113977.
[14] Y. Tan, X. Zhu, H. Wang, Y.W. Lv, Y.D. Ding, Q. Liao, A novel stacked rotary cup atomizer toward efficient centrifugal granulation of molten blast furnace slag, Steel Res. Int. 92 (2021) 2100207, https://doi.org/10.1002/srin.202100207.
[15] Y. Tan, X. Zhu, X.Y. He, B. Ding, H. Wang, Q. Liao, H. Li, Granulation characteristics of molten blast furnace slag by hybrid centrifugal-air blast technique, Powder Technol. 323 (2018) 176–185, https://doi.org/10.1016/j.powtec.2017.09.040.
[16] W.C. He, X.W. Lv, F.F. Pan, X.Q. Li, Z.M. Yan, Novel preparation process of iron powders with semisteel by rotary cup atomizer, Powder Technol. 356 (2019) 1087–1096, https://doi.org/10.1016/j.powtec.2019.09.009.
[17] W.C. He, X.W. Lv, F.F. Pan, L.Z. Gao, X.Q. Li, J. Qiu, Granulation of ferrosilicon alloy by rotary multi-nozzles cup atomizer: granulation behavior and model formation, Adv. Powder Technol. 30 (2019) 895–902, https://doi.org/10.1016/j.apt.2019.02.003.
[18] Y.H. Pan, M. Zhao, P. Ma, J. Li, Z.Y. Huo, H.Y. Li, CFD modeling of melt spreading behavior on spinning discs and cups for centrifugal granulation of molten slag, J. Sustain. Metall. 5 (2019) 195–203, https://doi.org/10.1007/s40831-019-00213-1.
[19] Y. Pan, P. Witt, J.B. Kuan, D. Xie, CFD modelling of the effects of operating parameters on the spreading of liquids on a spinning disc, J. Comput. Multiphase Flows. (2014) 49–64, https://doi.org/10.1260/1757-482X.6.1.49.
[20] D.X. Wang, X. Ling, H. Peng, Simulation of ligament mode breakup of molten slag by spinning disk in the dry granulation process, Appl. Therm. Eng. 84 (2015) 437–447, https://doi.org/10.1016/j.applthermaleng.2015.03.003.
[21] D.X. Wang, X. Ling, H. Peng, Theoretical analysis of free-surface film flow on the rotary granulating disk in waste heat recovery process of molten slag, Appl. Therm. Eng. 63 (2014) 387–395, https://doi.org/10.1016/j.applthermaleng.2013.11.033.
[22] Y.B. Li, X.S. Wu, Y.Z. Liu, G.W. Chu, B.C. Sun, Y. Luo, J.F. Chen, Three-dimensional large eddy simulation of wave characteristics of liquid film flow in a spinning disk reactor, AICHE J. 66 (2019), https://doi.org/10.1002/aic.16894.
[23] W.C. He, X.W. Lv, Z.M. Yan, G.Q. Fan, Ferrosilicon alloy granules prepared through centrifugal granulation process, J. Iron Steel Res. Int. 27 (2020) 1247–1258, https://doi.org/10.1007/s42243-020-00430-z.
[24] J. Gao, Y.H. Feng, W.X. Zhang, D.L. Feng, X.X. Zhang, Prediction on particle size characteristics of high-temperature liquid blast furnace slag in a centrifugal granulation process, Powder Technol. 376 (2020) 527–536, https://doi.org/10.1016/j.powtec.2020.08.033.

[25] J. Gao, Y.H. Feng, D.L. Feng, X.X. Zhang, Granulation performance by hybrid centrifugal-air blast technique for treatment of liquid slag, Powder Technol. 392 (2021) 204–211, https://doi.org/10.1016/j.powtec.2021.07.002.
[26] V.T. Mantripragada, K. Kumar, P. Kumar, S. Sarkar, Modeling of powder production during centrifugal atomization, J. Sustain. Metall. 7 (2021) 620–629, https://doi.org/10.1007/s40831-021-00370-2.
[27] M.Q. Li, J. Zhao, X. Zhang, N.W. Xu, H.Y. Meng, Z.Q. Wu, S.Z. Wang, Effects of granulator structure and cooperating mode with slag tube on the centrifugal granulation characteristics of molten slag, Appl. Therm. Eng. 193 (2021), 117026, https://doi.org/10.1016/j.applthermaleng.2021.117026.
[28] N.W. Xu, J. Zhao, X. Zhang, M.Q. Li, C. Ma, Z.Q. Wu, H.Y. Meng, S.Z. Wang, Flow characteristics of the liquid film during centrifugal granulation of liquid slag on the surface of rotary cup, J. Sustain. Metall (2022) 632–645, https://doi.org/10.1007/s40831-021-00438-z.
[29] L.L. Wang, Y.Z. Zhang, Y. Long, H.B. Ke, Simulation of primary breakup of molten slag in the gas quenching dry granulation process, Appl. Therm. Eng. 181 (2020), 115850, https://doi.org/10.1016/j.applthermaleng.2020.115850.
[30] Y. Feng, J. Gao, D. Feng, X. Zhang, Modeling of the molten blast furnace slag particle deposition on the wall including phase change and heat transfer, Appl. Energy 248 (2019) 288–298, https://doi.org/10.1016/j.apenergy.2019.04.100.
[31] Y.Y. Zhao, M.H. Jacobs, A.L. Dowson, Liquid flow on a rotating disk prior to centrifugal atomization and spray deposition, Metall. Mater. Trans. B Process Metall. Mater. Process. Sci. 29 (1998) 1357–1369, https://doi.org/10.1007/s11663-998-0059-1.
[32] R. Dhirhi, K. Prasad, A.K. Shukla, S. Sarkar, T. Renganathan, S. Pushpavanam, M. Kaza, Experimental study of rotating dry slag granulation unit: operating regimes, particle size analysis and scale up, Appl. Therm. Eng. 107 (2016) 898–906, https://doi.org/10.1016/j.applthermaleng.2016.07.049.
[33] Y. Min, J. Huang, C.J. Liu, M.F. Jiang, X.Q. Yu, Physical simulation of molten slag granulation by rotary disk, J. Iron Steel Res. Int. 20 (2013) 26–32, https://doi.org/10.1016/S1006-706X(13)60152-1.